Brief Communication | Pediatric Imaging

eISSN 2005-8330
https://doi.org/10.3348/kjr.2019.0689
Korean J Radiol 2020;21(6):717-725

Korean Journal of Radiology
KJR

Pattern Analysis of Left Ventricular Remodeling Using Cardiac Computed Tomography in Children with Congenital Heart Disease: Preliminary Results

Hyun Woo Goo, MD, PhD, Sang-Hyub Park, RT, BD

All authors: Department of Radiology and Research Institute of Radiology, University of Ulsan College of Medicine, Asan Medical Center, Seoul, Korea

Objective: To assess left ventricular remodeling patterns using cardiac computed tomography (CT) in children with congenital heart disease and correlate these patterns with their clinical course.

Materials and Methods: Left ventricular volume and myocardial mass were quantified in 17 children with congenital heart disease who underwent initial and follow-up end-systolic cardiac CT studies with a mean follow-up duration of 8.4 ± 9.7 months. Based on changes in the indexed left ventricular myocardial mass (LVMi) and left ventricular mass-volume ratio (LVMVR), left ventricular remodeling between the two serial cardiac CT examinations was categorized into one of four patterns: pattern 1, increased LVMi and increased LVMVR; pattern 2, decreased LVMi and decreased LVMVR; pattern 3, increased LVMi and decreased LVMVR; and pattern 4, decreased LVMi and increased LVMVR. Left ventricular remodeling patterns were correlated with unfavorable clinical courses.

Results: Baseline LVMi and LVMVR were 65.1 ± 37.9 g/m^2 and 4.0 ± 3.2 g/mL, respectively. LVMi increased in 10 patients and decreased in seven patients. LVMVR increased in seven patients and decreased in 10 patients. Pattern 1 was observed in seven patients, pattern 2 in seven, and pattern 3 in three patients. Unfavorable events were observed in 29% (2/7) of patients with pattern 1 and 67% (2/3) of patients with pattern 3, but no such events occurred in pattern 2 during the follow-up period (4.4 ± 2.7 years).

Conclusion: Left ventricular remodeling patterns can be characterized using cardiac CT in children with congenital heart disease and may be used to predict their clinical course.

Keywords: *Cardiac CT; Congenital heart disease; Cardiac volumetric quantification; Left ventricular remodeling; Left ventricular hypertrophy; Threshold-based segmentation*

INTRODUCTION

Left ventricular hypertrophy (LVH) is a critical factor predicting adverse cardiovascular events such as arrhythmia, heart failure, and sudden cardiac death (1). However, LVH may be a beneficial compensatory reaction to left ventricular wall stress. To analyze the various patterns of left ventricular remodeling (LVR), it is important to consider changes in ventricular volume in addition to myocardial mass. LVR is largely divided into adaptive and maladaptive patterns. LVR caused by pressure and/or volume overload has been studied in patients with aortic valvular disease (2-4), but has rarely been reported in patients with congenital heart disease, except for congenitally corrected transposition of the great arteries before and after pulmonary artery banding to prepare the left ventricle in systemic circulation following subsequent anatomic repair (5-7). Cardiac magnetic resonance imaging (MRI) has been used to overcome inherent limitations of

Received: September 14, 2019 **Revised:** November 24, 2019
Accepted: February 9, 2020
Corresponding author: Hyun Woo Goo, MD, PhD, Department of Radiology and Research Institute of Radiology, University of Ulsan College of Medicine, Asan Medical Center, 88 Olympic-ro 43-gil, Songpa-gu, Seoul 05505, Korea.
• Tel: (822) 3010-4388 • Fax: (822) 476-0090
• E-mail: ghw68@hanmail.net

echocardiography with respect to geometric assumptions, acoustic window, and operator dependency, and to provide a better evaluation of LVR in patients with aortic stenosis (8). Accuracy and reproducibility of quantification are greatly influenced by the segmentation method for left ventricular volume and more greatly for myocardial mass (9, 10). Generally, threshold-based segmentation, which includes the papillary muscles and trabeculations in the myocardial mass, is superior to the simplified contouring method (11). In addition, a three-dimensional (3D) version of threshold-based segmentation is desirable to reduce errors associated with a two-dimensional version (12). Recently, a semiautomatic 3D threshold-based segmentation method with high reproducibility was successfully applied to 3D cardiac computed tomography (CT) datasets, not only for ventricular volume measurement in patients with congenital heart disease (13-17), but also for left ventricular myocardial mass quantification in patients with various degrees of LVH (18). However, LVR that considers both volume and mass has not been evaluated with cardiac CT and 3D threshold-based segmentation. Therefore, we aimed to assess LVR patterns using cardiac CT in children with congenital heart disease and correlate these patterns with their clinical course.

MATERIALS AND METHODS

This retrospective study was approved by the local Institutional Review Board and the requirement for informed consent was waived.

Study Population

Between June 2011 and August 2016, 17 patients with congenital heart disease (median age at the first cardiac CT, 22 days; range, 2 days to 16 years; male:female = 10:7) underwent initial and follow-up electrocardiography (ECG)-synchronized end-systolic cardiac CT examinations (time interval, 8.4 ± 9.7 months) using a second-generation dual-source scanner (SOMATOM Definition Flash; Siemens Healthineers, Forchheim, Germany). Therefore, 34 cardiac

Table 1. Demographic Characteristics, Diagnosis, and Treatment of Study Population

Case Number	Sex	Age at 1st Cardiac CT	Time Interval between Serial CT Examinations	Diagnosis and Previous Treatment	Interval Treatment
1	M	2 days	19 days	TGA, VSD, S/P BAS	Arterial switch operation
2	M	2 days	82 days	HLHS variant, CoA	Bilateral PAB
3	F	4 days	895 days	CoA	Arch repair
4	M	6 days	378 days	CoA	Arch repair
5	M	7 days	361 days	CoA	Arch repair
6	M	15 days	357 days	IAA, VSD, S/P arch repair	N/A
7	F	16 days	349 days	CoA	Arch repair
8	F	20 days	436 days	Critical aortic stenosis, S/P Sano modified Norwood operation	Pulmonary artery angioplasty, right modified Blalock-Taussig shunt
9	F	22 days	77 days	IAA, VSD, S/P arch repair	N/A
10	M	1 month	344 days	CoA	Arch repair
11	M	8 months	98 days	Congenially-corrected TGA with intact ventricular septum, S/P PAB	N/A
12	M	8 months	161 days	Large ASD, BPD, pulmonary hypertension	Sutureless repair, ASD closure
13	F	17 months	99 days	Williams syndrome	Modified sliding aortoplasty
14	M	9 years	82 days	Williams syndrome	Aortoplasty, bypass graft
15	F	10 years	31 days	TGA, VSD, tricuspid atresia, S/P Fontan operation	VSD extension, mitral valvuloplasty
16	F	10 years	929 days	CoA	N/A
17	M	16 years	19 days	Bicuspid aortic valve, aortic regurgitation	Bentall operation

ASD = atrial septal defect, BAS = balloon atrial septostomy, BPD = bronchopulmonary dysplasia, CoA = coarctation of aorta, CT = computed tomography, F = female, HLHS = hypoplastic left heart syndrome, IAA = interrupted aortic arch, M = male, N/A = not applicable, PAB = pulmonary artery banding, S/P = status post, TGA = transposition of great arteries, VSD = ventricular septal defect

https://doi.org/10.3348/kjr.2019.0689

Korean Journal of Radiology
KJR

CT examinations were included in this study. Demographic characteristics, diagnosis, and treatment of the study population are described in Table 1. The median time interval between the most recent surgical or interventional treatment and the first CT study available in 47.1% (8/17) of the patients was 27 days (range, 1 day–8.8 years), and the median time between the most recent surgical or interventional treatment and the follow-up CT study available in all patients was 0.9 years (range, 7 days–9.0 years). The body surface area (m^2) on cardiac CT was used to index volumetric measurements.

Cardiac CT

The fundamental scan parameters of the cardiac CT were as follows: 2 x 64 x 0.6-mm slices with the z-flying focal spot technique; gantry rotation time, 0.28 seconds; temporal resolution, 75 ms; slice width, 0.75 mm; and reconstruction interval, 0.4 mm. Scan protocols were further optimized to minimize radiation dose and maintain diagnostic image quality (19-26). For ECG-synchronized data acquisition, a breath-hold retrospectively ECG-gated spiral scan was used in 8 examinations; free-breathing combined prospectively ECG- and respiratory-triggered sequential scan in 13, and free-breathing prospectively ECG-triggered sequential scan in 13. Of the free-breathing children, respiratory triggering was added to ECG-triggered sequential scanning in patients weighing > 5 kg in whom respiratory motion was large enough to degrade the image quality of the cardiac CT; a pressure-sensing belt from a respiratory gating system (AZ-733V; Anzai Medical Co, Tokyo, Japan) was used to obtain respiratory triggering as previously described (27). For sedation, children (usually younger than 6 years of age) were initially given oral chloral hydrate (50 mg/kg) followed by administration of intravenous midazolam (0.1 mg/kg) or ketamine (1 mg/kg) as required. The lowest possible tube voltage was selected for greater radiation dose efficiency and iodine contrast-to-noise ratio; 70 kV was used in 17 examinations, 80 kV in 13, and 100 kV in four.

Iodinated contrast agent (Iomeron 400, iomeprol 400 mg I/mL; Bracco Imaging SpA, Milan, Italy; 1.5–2.0 mL/kg) was administered intravenously using a dual-head power injector at an injection rate of 0.3–3.0 mL/s. A tri-phasic or quadri-phasic injection protocol was utilized to achieve uniform cardiovascular enhancement and minimal peri-venous streak artifacts from undiluted contrast agent. The scan delay time was determined using a bolus tracking technique with a trigger threshold of 150 HU in the left ventricular cavity.

Volume CT dose index and dose-length product values based on a 32-cm phantom were 3.5 ± 4.7 mGy and 60.6 ± 98.8 mGy·cm, respectively. The effective dose value of cardiac CT calculated by multiplying the dose-length product by the age, sex, and tube voltage-specific conversion factors was 1.2 ± 1.4 mSv (28, 29).

Quantification of Left Ventricular Volumetric Parameters

Left ventricular end-systolic cavity volume and myocardial mass were quantified by using a commercially available workstation (Advantage Workstation 4.6; GE Healthcare, Milwaukee, WI, USA). First, the epicardial border of the left ventricle was delineated consecutively using one-click identification of the left ventricle, a 3D region-growing method, and manual adjustment. The mitral and aortic valve planes were then defined manually. For the total volume of the left ventricle, the left ventricular cavity volume was separated from the left ventricular myocardial volume by using 3D threshold-based segmentation. The left ventricular myocardial mass (in grams) was calculated by multiplying the specific gravity of the myocardium (1.05 g/mL or g/cm^3) by the quantified myocardial volume. Left ventricular mass-volume ratio (LVMVR) was calculated by dividing the left ventricular myocardial mass by the left ventricular volume. The left ventricular volume and myocardial mass were indexed to body surface area. Based on a previous article using the same segmentation method, the indexed left ventricular myocardial mass (LVMi) was categorized as either no hypertrophy (< 60.2 g/m^2), borderline hypertrophy (60.2–74.0 g/m^2), or definite hypertrophy (≥ 74.1 g/m^2) (18).

Left Ventricular Overload

Left ventricular overloaded conditions in each patient were characterized based on the following echocardiographic and cardiac CT findings: pressure overload was regarded present when substantial obstruction was observed in the aortic arch (pressure gradient ≥ 20 mm Hg), aortic valve (≥ 36 mm Hg), or left ventricular outflow tract (≥ 30 mm Hg), or when the aortic valve annulus was small (Z score < -2). Volume overload was considered present when aortic or mitral regurgitation greater than grade 2 (or moderate) was observed, or when right-to-left or bidirectional shunt flow through a ventricular septal defect was identified.

Patterns of Left Ventricular Remodeling

Based on changes in LVMi and LVMVR between the two

 https://doi.org/10.3348/kjr.2019.0689

serial cardiac CT examinations, LVR was categorized into one of four patterns: pattern 1, increased LVMi and increased LVMVR (Fig. 1); pattern 2, decreased LVMi and decreased LVMVR (Fig. 2); pattern 3, increased LVMi and decreased LVMVR (Fig. 3); and pattern 4, decreased LVMi and increased LVMVR.

Clinical Courses

All patients were followed up (4.4 ± 2.7 years) to determine whether an unfavorable event had occurred, such as re-operation or re-intervention for a residual lesion causing left ventricular pressure or volume overload, application of extracorporeal membrane oxygenation, left

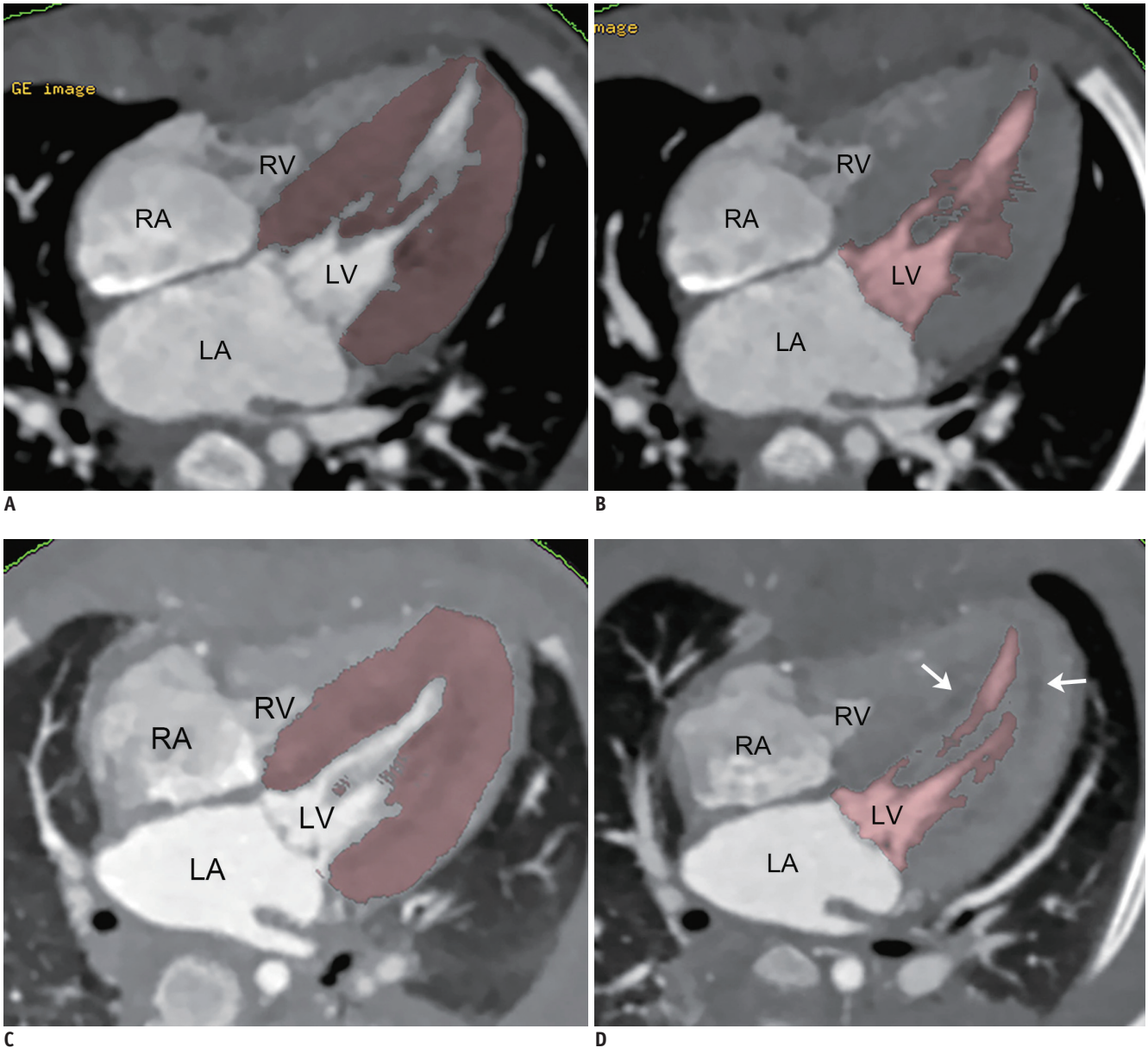

Fig. 1. 17-month-old girl with Williams syndrome demonstrating pattern 1 of left ventricular remodeling.
Four-chamber views of initial **(A, B)** and follow-up **(C, D)** end-systolic cardiac CT examinations show segmented left ventricular myocardium **(A, C)** and cavity **(B, D)** in pink. Diffuse subendocardial hypodense lesions (arrows) are noted in left ventricular myocardium on follow-up cardiac CT **(D)**. She underwent modified sliding aortoplasty between two CT examinations. During interval of 99 days, indexed left ventricular myocardial mass increased from 62.5 g/m^2 to 73.5 g/m^2 and left ventricular mass-volume ratio also increased from 4.1 g/mL to 5.4 g/ml. In contrast, indexed left ventricular end-systolic volume decreased slightly from 14.4 mL/m^2 to 13.0 mL/m^2 during same period. She had left ventricular volume overload due to greater than grade 2 mitral regurgitation and experienced unfavorable events, including left ventricular dysfunction, myocardial infarction, and application of extracorporeal membrane oxygenation during follow-up period of 4.3 years. LA = left atrium, LV = left ventricle, RA = right atrium, RV = right ventricle

https://doi.org/10.3348/kjr.2019.0689

Korean Journal of Radiology
KJR

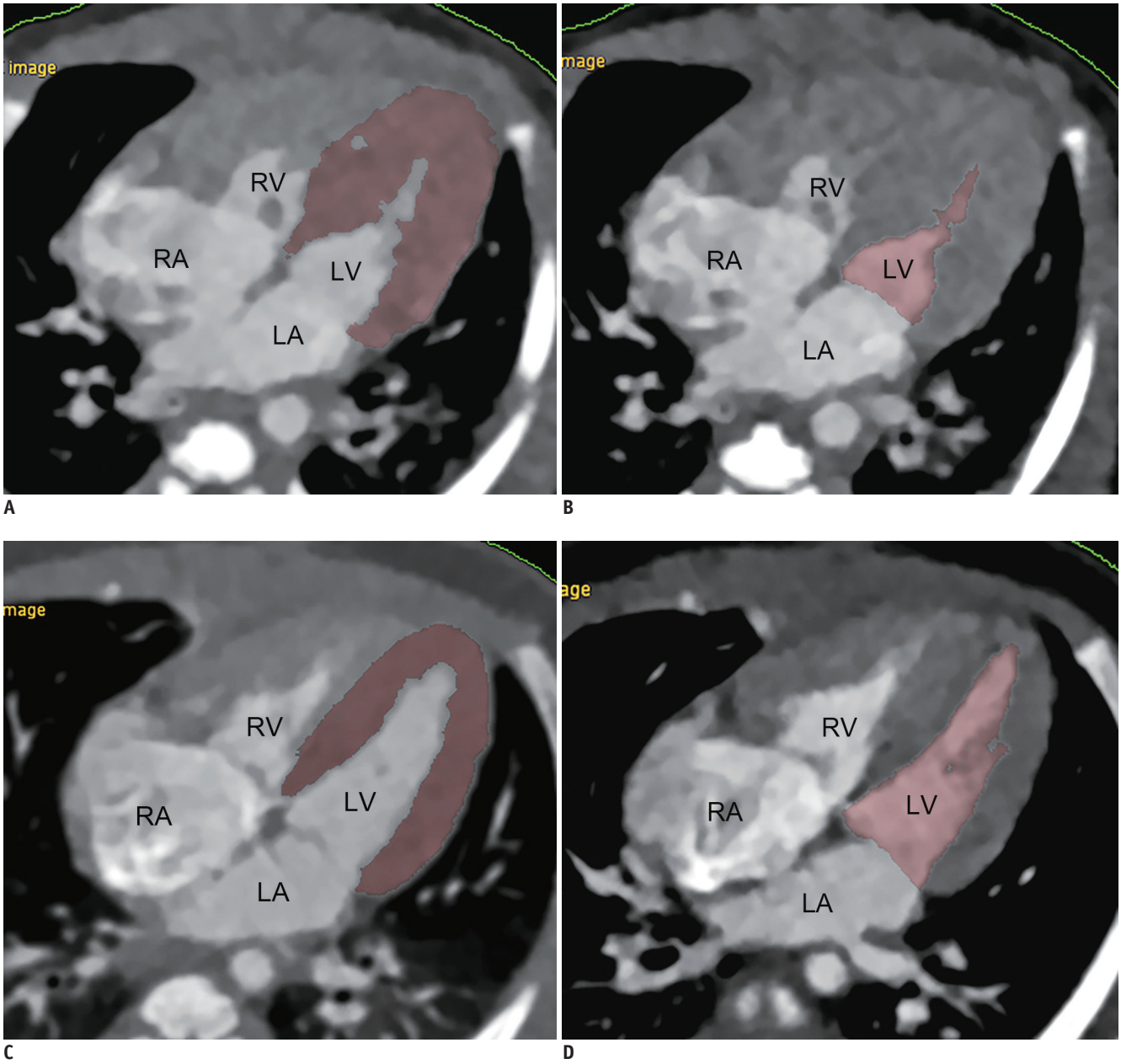

Fig. 2. 22-day-old girl with repaired interrupted aortic arch and ventricular septal defect demonstrating pattern 2 of left ventricular remodeling.

Four-chamber views of initial **(A, B)** and follow-up **(C, D)** end-systolic cardiac CT examinations show segmented left ventricular myocardium **(A, C)** and cavity **(B, D)** in pink. During interval of 77 days between two CT examinations, indexed left ventricular myocardial mass markedly decreased from 53.6 g/m^2 to 36.0 g/m^2 and left ventricular mass-volume ratio also strikingly decreased from 8.9 g/mL to 2.6 g/mL. In contrast, indexed left ventricular end-systolic volume greatly increased from 6.0 mL/m^2 to 13.7 mL/m^2 for same period. She had small aortic valve annulus below Z score of -3, and never experienced unfavorable events during follow-up period of 2.6 years.

ventricular dysfunction, myocardial infarction, arrhythmia, heart failure, or cardiac death.

Data Analysis

Continuous variables are presented as mean ± standard deviation or median with range, and categorical variables are expressed as frequency with percentage. To explore their clinical significance, LVR patterns were correlated with unfavorable clinical courses. Descriptive data analyses were performed using Excel (Microsoft Corp., Redmond, WA, USA).

https://doi.org/10.3348/kjr.2019.0689

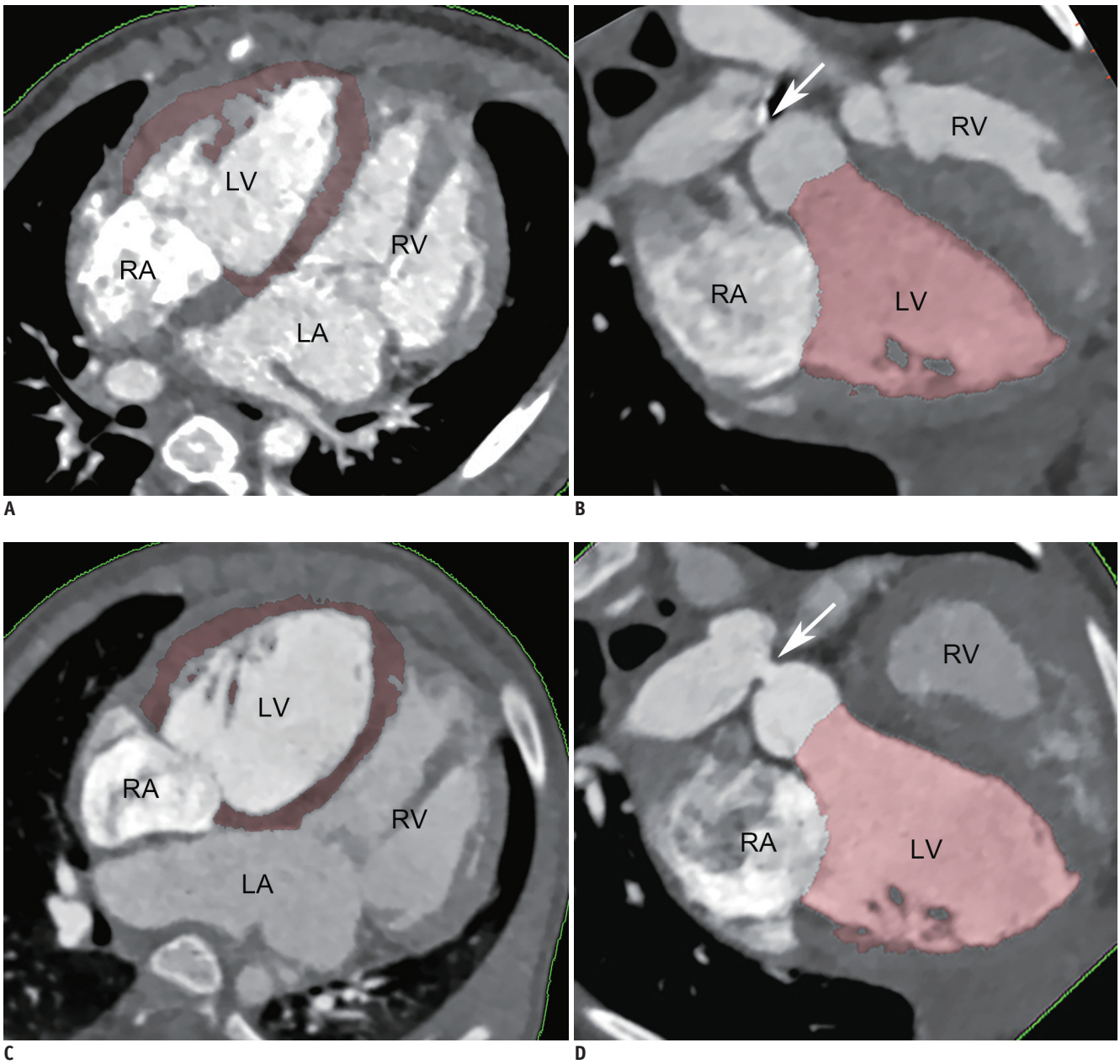

Fig. 3. 8-month-old boy with congenitally corrected transposition of great arteries and intact ventricular septum, who underwent pulmonary artery banding for left ventricle preparation, demonstrating pattern 3 of left ventricular remodeling.
Four-chamber views **(A, C)** and left ventricular vertical long-axis views **(B, D)** of initial **(A, B)** and follow-up **(C, D)** end-systolic cardiac CT examinations show segmented left ventricular myocardium **(A, C)** and cavity **(B, D)** in pink. During interval of 98 days between two CT examinations, indexed left ventricular myocardial mass slightly increased from 72.2 g/m^2 to 77.6 g/m^2 and indexed left ventricular end-systolic volume markedly increased from 66.9 mL/m^2 to 119.3 mL/m^2. In contrast, left ventricular mass-volume ratio decreased from 1.0 g/mL to 0.6 g/mL during same period. He had left ventricular pressure overload due to pulmonary artery banding (arrows) and experienced unfavorable events, including left ventricular dysfunction, arrhythmia, and cardiac death during follow-up period of 0.8 years. Interventricular septum appears convex towards RV **(A, C)**, suggesting supra-systemic left ventricular pressure at end-systole. Enlarged RV and LA were noted.

RESULTS

Left Ventricular Volumetric Parameters

The mean baseline LVMi and LVMVR in 17 patients were 65.1 ± 37.9 g/m^2 and 4.0 ± 3.2 g/mL, respectively. Of 34 examinations, LVMi showed no hypertrophy in 20, borderline hypertrophy in eight, and definite hypertrophy in six. There was no change in the degree of LVH between serial examinations in 14 patients, but 3 patients showed a change in category. LVMi increased from 52.2 ± 39.0 g/m^2

https://doi.org/10.3348/kjr.2019.0689

Korean Journal of Radiology
KJR

Table 2. Correlation between Patterns of Left Ventricular Remodeling and Unfavorable Clinical Course

Left Ventricular Remodeling Patterns	LVMi	LVMVR	No. of Cases	Pressure Overload	Volume Overload	Unfavorable Events	Follow-Up Period (Years)
Pattern 1	Increased	Increased	7	57% (4/7)	29% (2/7)	29% (2/7)	2.5–8.2
Pattern 2	Decreased	Decreased	7	57% (4/7)	14% (1/7)	0% (0/5)	1.1–8.2
Pattern 3	Increased	Decreased	3	100% (3/3)	33% (1/3)	67% (2/3)	0.8–8.3

LVMi = indexed left ventricular myocardial mass, LVMVR = left ventricular mass-volume ratio

at the initial CT to 70.4 ± 33.1 g/m^2 at the follow-up CT in 10 patients during the interval of 0.9 ± 1.0 years, whereas LVMi decreased from 77.9 ± 42.8 g/m^2 at the initial CT to 63.1 ± 40.5 g/m^2 at the follow-up CT in 7 patients during the interval of 0.5 ± 0.4 years. On the other hand, LVMVR increased from 2.1 ± 1.1 g/mL at the initial CT to 3.4 ± 1.1 g/mL at the follow-up CT in 7 patients during the interval of 0.9 ± 1.1 years, while LVMVR decreased from 6.6 ± 4.4 g/mL at the initial CT to 3.0 ± 2.6 g/mL at the follow-up CT in 10 patients during the interval of 0.6 ± 0.4 years.

Left Ventricular Overload

Of 17 patients, pressure overload was present in 11 patients (aortic arch obstruction in six, a small aortic valve annulus in three, left ventricular outflow obstruction in two, aortic valve stenosis in one, and pulmonary artery banding in one), and two kinds of pressure overload were identified in two patients. Of 17 patients, volume overload was present in four patients (mitral regurgitation in two, aortic regurgitation in one, and shunt through a ventricular septal defect in one). Two patients had a combination of pressure and volume overload.

Correlation between Patterns of Left Ventricular Remodeling and Unfavorable Clinical Course

Patterns of LVR are summarized in Table 2. Pattern 1 was observed in seven patients (Fig. 1), pattern 2 in seven (Fig. 2), and pattern 3 in three patients (Fig. 3). No patient was categorized into pattern 4. Unfavorable events were identified in four patients (left ventricular dysfunction in three, application of extracorporeal membrane oxygenation in two, cardiac death in two, myocardial infarction in one, and arrhythmia in one) with multiple events in three patients. Unfavorable events were observed in 29% (2/7) of patients with pattern 1 and 67% (2/3) of patients with pattern 3, but no such events occurred in patients with pattern 2 during the follow-up period.

DISCUSSION

This study demonstrated that LVR patterns could be characterized using cardiac CT in children with congenital heart disease, and the patterns were used to predict clinical course. Based on the preliminary results of this study, the most favorable clinical course was observed in pattern 2 (decreased LVMi and LVMVR), the most unfavorable clinical course in pattern 3 (increased LVMi and decreased LVMVR), and the clinical course in pattern 1 (increased LVMi and LVMVR) was intermediate between the two extremes.

LVH is an adaptive reaction to pressure overloaded conditions that increase left ventricular wall stress to maintain cardiac performance despite the elevated left ventricular systolic pressure, but is associated with excess cardiac mortality and morbidity (3). Notably, incomplete regression of LVH is associated with decreased survival and regarded as a maladaptive response leading to left ventricular diastolic dysfunction (30). To analyze LVR patterns to pressure and/or volume overloaded conditions, LVMi and LVMVR were utilized to consider left ventricular volume in addition to myocardial mass in this study. For example, an increase in left ventricular volume and maintenance of relatively normal LVMVR is generally regarded a hallmark of compensatory hypertrophy. In fact, LVMVR has commonly been used to evaluate LVR and increased LVMVR (i.e., concentric LVH) is associated with a hypertensive response to exercise in patients with repaired coarctation of the aorta (31).

Favorable LVR occurs as a regression process after the relief of overloaded conditions. In a previous study using cardiac MRI (2), it was characterized by a decrease in both LVMi and LVMVR, with an improvement in diastolic filling in patients with aortic valve stenosis early (approximately 9 months) after aortic valve replacement (2). This LVR is comparable to pattern 2 demonstrated in this study.

As previously mentioned, LVH may develop as a compensatory remodeling process (5). After pulmonary artery banding in transposition of the great arteries,

 https://doi.org/10.3348/kjr.2019.0689

serial increases in both LVMi and LVMVR as measured using echocardiography or cardiac MRI indicate that the increment of myocardial mass is disproportionately greater than that of ventricular volume (5, 6). This remodeling pattern is analogous to pattern 1 in this study, showing an intermediate clinical outcome between patterns 2 and 3.

Maladaptive LVR may produce patterns 3 or 4. Pattern 3 is characterized by a disproportionally greater increase in ventricular volume than that in myocardial mass, resulting in a reduction in LVMVR. In contrast, pattern 4 is characterized by a disproportionally greater decrease in ventricular volume than that in myocardial mass, leading to increased LVMVR. In this study, a poor clinical outcome frequently occurred in pattern 3. Pattern 4 was observed in patients with aortic regurgitation after aortic valve replacement (2).

The same strategy as that used in this study may be applied to characterize right ventricular remodeling patterns in response to severe pulmonary regurgitation in patients with repaired tetralogy of Fallot and other congenital heart diseases, mainly involving the right ventricle (32). Myocardial fibrosis is responsible for late diastolic dysfunction that slowly normalizes or persists after treatment in patients with LVH (3, 4). Therefore, the evaluation of myocardial fibrosis using late gadolinium enhancement MRI (33), T1 mapping with extracellular volume map (34), or myocardial delayed-enhancement CT (35), has an additional prognostic value in analyzing LVR.

Retrospective study design and the small study population are major limitations of this study. Its retrospective nature might lead to selection bias in which more severe cases were enrolled in the study population. Moreover, statistical and subgroup analyses were limited due to the small number of patients with variable patient age and pathology. The time intervals between serial cardiac CT examinations were also highly variable. Pathology-based verification of left ventricular mass quantification using 3D CT data is practically impossible. Nonetheless, the same 3D threshold-based approach as used in this study previously demonstrated high reproducibility with a mean difference between the two evaluation sessions of 2.3 ± 1.1% (18). To validate the clinical utility of the CT-based pattern analysis of LVR demonstrated in this study, further studies are necessary. Prospective studies will be particularly valuable to prove its clinical value. Optimal timing of the evaluation and further divisions of LVR patterns remain to be determined. Nevertheless, the results of this study could unveil the great potential of CT-based pattern analysis of LVR in predicting clinical outcomes.

In conclusion, LVR patterns can be characterized using cardiac CT in children with congenital heart disease and may be used to predict their clinical course.

Conflicts of Interest

The authors have no potential conflicts of interest to disclose.

ORCID iD

Hyun Woo Goo
https://orcid.org/0000-0001-6861-5958

REFERENCES

1. Stevens SM, Reinier K, Chugh SS. Increased left ventricular mass as a predictor of sudden cardiac death: is it time to put it to the test? *Circ Arrhythm Electrophysiol* 2013;6:212-217
2. Lamb HJ, Beyerbacht HP, de Roos A, van der Laarse A, Vliegen HW, Leujes F, et al. Left ventricular remodeling early after aortic valve replacement: differential effects on diastolic function in aortic valve stenosis and aortic regurgitation. *J Am Coll Cardiol* 2002;40:2182-2188
3. Villa E, Troise G, Cirillo M, Brunelli F, Tomba MD, Mhagna Z, et al. Factors affecting left ventricular remodeling after valve replacement for aortic stenosis. An overview. *Cardiovasc Ultrasound* 2006;4:25
4. Yarbrough WM, Mukherjee R, Ikonomidis JS, Zile MR, Spinale FG. Myocardial remodeling with aortic stenosis and after aortic valve replacement: mechanisms and future prognostic implications. *J Thorac Cardiovasc Surg* 2012;143:656-664
5. Boutin C, Jonas RA, Sanders SP, Wernovsky G, Mone SM, Colan SD. Rapid two-stage arterial switch operation. Acquisition of left ventricular mass after pulmonary artery banding in infants with transposition of the great arteries. *Circulation* 1994;90:1304-1309
6. Myers PO, del Nido PJ, Geva T, Bautista-Hernandez V, Chen P, Mayer JE Jr, et al. Impact of age and duration of banding on left ventricular preparation before anatomic repair for congenitally corrected transposition of the great arteries. *Ann Thorac Surg* 2013;96:603-610
7. Moodley S, Balasubramanian S, Tacy TA, Chan F, Hanley FL, Punn R. Echocardiography-derived left ventricular outflow tract gradient and left ventricular posterior wall thickening are associated with outcomes for anatomic repair in congenitally corrected transposition of the great arteries. *J Am Soc Echocardiogr* 2017;30:807-814
8. Dweck MR, Joshi S, Murigu T, Gulati A, Alpendurada F, Jabbour A, et al. Left ventricular remodeling and hypertrophy in patients with aortic stenosis: insights from cardiovascular magnetic resonance. *J Cardiovasc Magn Reson* 2012;14:50

https://doi.org/10.3348/kjr.2019.0689

9. Han Y, Osborn EA, Maron MS, Manning WJ, Yeon SB. Impact of papillary and trabecular muscles on quantitative analyses of cardiac function in hypertrophic cardiomyopathy. *J Magn Reson Imaging* 2009;30:1197-1202
10. Miller CA, Jordan P, Borg A, Argyle R, Clark D, Pearce K, et al. Quantification of left ventricular indices from SSFP cine imaging: impact of real-world variability in analysis methodology and utility of geometric modeling. *J Magn Reson Imaging* 2013;37:1213-1222
11. Varga-Szemes A, Muscogiuri G, Schoepf UJ, Wichmann JL, Suranyi P, De Cecco CN, et al. Clinical feasibility of a myocardial signal intensity threshold-based semi-automated cardiac magnetic resonance segmentation method. *Eur Radiol* 2016;26:1503-1511
12. Sugeng L, Mor-Avi V, Weinert L, Niel J, Ebner C, Steringer-Mascherbauer R, et al. Multimodality comparison of quantitative volumetric analysis of the right ventricle. *JACC Cardiovasc Imaging* 2010;3:10-18
13. Kim HJ, Goo HW, Park SH, Yun TJ. Left ventricle volume measured by cardiac CT in an infant with a small left ventricle: a new and accurate method in determining uni- or biventricular repair. *Pediatr Radiol* 2013;43:243-246
14. Goo HW, Park SH. Semiautomatic three-dimensional CT ventricular volumetry in patients with congenital heart disease: agreement between two methods with different user interaction. *Int J Cardiovasc Imaging* 2015;31 Suppl 2:223-232
15. Goo HW. Serial changes in anatomy and ventricular function on dual-source cardiac computed tomography after the Norwood procedure for hypoplastic left heart syndrome. *Pediatr Radiol* 2017;47:1776-1786
16. Goo HW, Park SH. Computed tomography-based ventricular volumes and morphometric parameters for deciding the treatment strategy in children with a hypoplastic left ventricle: preliminary results. *Korean J Radiol* 2018;19:1042-1052
17. Goo HW. Semiautomatic three-dimensional threshold-based cardiac computed tomography ventricular volumetry in repaired tetralogy of Fallot: comparison with cardiac magnetic resonance imaging. *Korean J Radiol* 2019;20:102-113
18. Goo HW. Technical feasibility of semiautomatic three-dimensional threshold-based cardiac computed tomography quantification of left ventricular mass. *Pediatr Radiol* 2019;49:318-326
19. Goo HW, Suh DS. Tube current reduction in pediatric non-ECG-gated heart CT by combined tube current modulation. *Pediatr Radiol* 2006;36:344-351
20. Goo HW. State-of-the-art CT imaging techniques for congenital heart disease. *Korean J Radiol* 2010;11:4-18
21. Goo HW. Individualized volume CT dose index determined by cross-sectional area and mean density of the body to achieve uniform image noise of contrast-enhanced pediatric chest CT obtained at variable kV levels and with combined tube current modulation. *Pediatr Radiol* 2011;41:839-847
22. Goo HW. Is it better to enter a volume CT dose index value before or after scan range adjustment for radiation dose optimization of pediatric cardiothoracic CT with tube current modulation? *Korean J Radiol* 2018;19:692-703
23. Goo HW. Comparison of chest pain protocols for electrocardiography-gated dual-source cardiothoracic CT in children and adults: the effect of tube current saturation on radiation dose reduction. *Korean J Radiol* 2018;19:23-31
24. Hong SH, Goo HW, Maeda E, Choo KS, Tsai IC; Asian Society of Cardiovascular Imaging Congenital Heart Disease Study Group. User-friendly vendor-specific guideline for pediatric cardiothoracic computed tomography provided by the Asian Society of Cardiovascular Imaging Congenital Heart Disease Study Group: part 1. Imaging techniques. *Korean J Radiol* 2019;20:190-204
25. Tricarico F, Hlavacek AM, Schoepf UJ, Ebersberger U, Nance JW Jr, Vliegenthart R, et al. Cardiovascular CT angiography in neonates and children: image quality and potential for radiation dose reduction with iterative image reconstruction techniques. *Eur Radiol* 2013;23:1306-1315
26. Lee KB, Goo HW. Quantitative image quality and histogram-based evaluations of an iterative reconstruction algorithm at low-to-ultralow radiation dose levels: a phantom study in chest CT. *Korean J Radiol* 2018;19:119-129
27. Goo HW. Combined prospectively electrocardiography- and respiratory-triggered sequential cardiac computed tomography in free-breathing children: success rate and image quality. *Pediatr Radiol* 2018;48:923-931
28. Goo HW. CT radiation dose optimization and estimation: an update for radiologists. *Korean J Radiol* 2012;13:1-11
29. Lee E, Goo HW, Lee JY. Age- and gender-specific estimates of cumulative CT dose over 5 years using real radiation dose tracking data in children. *Pediatr Radiol* 2015;45:1282-1292
30. Gaasch WH, Carroll JD, Levine HJ, Criscitiello MG. Chronic aortic regurgitation: prognostic value of left ventricular end-systolic dimension and end-diastolic radius/thickness ratio. *J Am Coll Cardiol* 1983;1:775-782
31. Krieger EV, Clair M, Opotowsky AR, Landzberg MJ, Rhodes J, Powell AJ, et al. Correlation of exercise response in repaired coarctation of the aorta to left ventricular mass and geometry. *Am J Cardiol* 2013;111:406-411
32. Geva T. Repaired tetralogy of Fallot: the roles of cardiovascular magnetic resonance in evaluating pathophysiology and for pulmonary valve replacement decision support. *J Cardiovasc Magn Reson* 2011;13:9
33. Fine NM, Tandon S, Kim HW, Shah DJ, Thompson T, Drangova M, et al. Validation of sub-segmental visual scoring for the quantification of ischemic and nonischemic myocardial fibrosis using late gadolinium enhancement MRI. *J Magn Reson Imaging* 2013;38:1369-1376
34. Broberg CS, Chugh SS, Conklin C, Sahn DJ, Jerosch-Herold M. Quantification of diffuse myocardial fibrosis and its association with myocardial dysfunction in congenital heart disease. *Circ Cardiovasc Imaging* 2010;3:727-734
35. Goo HW. Myocardial delayed-enhancement CT: initial experience in children and young adults. *Pediatr Radiol* 2017;47:1452-1462

 https://doi.org/10.3348/kjr.2019.0689